Biomedical Engineering, Vol. 42, No. 6, 2008, pp. 273-279. Translated from Meditsinskaya Tekhnika, Vol. 42, No. 6, 2008, pp. 1-7.
Original article submitted June 27, 2008.

Research, Design, and Technology

Hardware–Software System for Noninvasive Electrocardiographic Heart Examination Based on Inverse Problem of Electrocardiography

L. A. Bokeriya, A. Sh. Revishvili, A. V. Kalinin*, V. V. Kalinin, O. A. Lyadzhina, and E. A. Fetisova

1. Introduction

Cardiac arrhythmia is an important cause of decrease in life quality and duration. Cardiac arrhythmias are serious medical and social problems. Success in the treatment of cardiac arrhythmia depends on the quality of diagnosis. Electrophysiological mechanism of cardiac arrhythmia and localization of arrhythmogenic substrates are very important for intervention and surgical methods of treatment of cardiac arrhythmia [2].

Invasive electrophysiological examination (EPE) of the heart is the main method of topical and electrophysiological diagnosis of cardiac arrhythmia. EPE is based on direct detection of electrocardiograms at the endocardial or epicardial surface of the heart (endocardial or epicardial mapping). Endocardial or epicardial mapping requires detectors to be inserted into the heart chambers or pericardial cavity. Because of invasive character of endocardial or epicardial mapping, this procedure should be performed immediately before incision antiarrhythmia treatment of myocardium within the framework of integral surgical or intervention treatment.

Development of a noninvasive method for EPE of the heart is an urgent problem. The method should provide electrophysiological information of the same diagnostic quality as endocardial or epicardial mapping. This method would significantly increase safety and availability of accurate diagnosis of cardiac arrhythmia. Noninvasive EPE of the heart should be included into the program of pre-surgical examination, which decreases the time of intra-operation search of the source of cardiac arrhythmia and reduces radiation load on the patient and medical personnel.

Methods based on inverse problem of electrocardiography (IP ECG) are very promising directions in noninvasive electrocardiography of the heart. In terms of potentials, IP ECG is called the problem of numerical reconstruction of potential of electric field of the heart at the epicardial surface from synchronous ECG detection at the thoracic cavity surface [1, 11].

IP ECG was first introduced in the 1970-1980s [1, 9]. Results obtained by group of Prof. Y. Rudy at the University of Washington provided an important step in the development of IP ECG. This group developed the method of noninvasive electrocardiographic imaging (ECGI) [12]. A group of researchers from University of Innsbruck developed a similar method of noninvasive imaging of cardiac electrophysiology (NICE) [10].

In spite of substantial progress in this direction, the problem of development of effective methods of solution of the inverse problem of electrocardiography remains urgent. Upgrade of electrophysiological diagnosis methods based on the inverse problem of electrocardiography is still an urgent problem.

In 2006-2007, a modern hardware–software system for noninvasive electrocardiographic examination of heart was developed at Bakulev Research Center for Cardiovascular Surgery, Russian Academy of Medical Sciences, Moscow. This system is based on the inverse problem of electrocardiography. This system has been clinically tested. In contrast to previous models, this system implements more advanced mathematical algorithms, which increases the accuracy of reconstruction of electric field of the heart [4].

The goal of this work was to describe the physical and mathematical aspects of IP ECG and algorithms of IP ECG, architecture of the hardware–software system, and first results of its clinical application.

Bakulev Research Center for Cardiovascular Surgery, Russian Academy of Medical Sciences, Moscow, Russia; E-mail: alec.kalinin@gmail.com; vitkv@list.ru
* To whom correspondence should be addressed.

2. Mathematical Aspects of Inverse Problem of Electrocardiography

The following model is used in IP ECG. The thoracic cavity is a second order conductor with linear conductance (independent of electric field potential). This conductor is limited by surrounding medium (air). Electric field of the heart is described within the framework of electrodynamics of steady-state currents in immobile media. Primary sources of electric field in the space between the thoracic cavity and epicardial heart surface are absent. Normal component of electric field strength is negligible at the chest surface because of the presence of conductor/air interface [7].

Let us consider mathematical aspects of this problem. Let $\Omega \in R^3$ be a component of thoracic cavity limited by smooth border $\partial\Omega$ including body surface contacting with surrounding medium B_S. The cross-sections of the thoracic cavity at the level of the diaphragm and clavicle B_{T1} and B_{T2}, as well as epicardial surface of the heart B_E, are also incorporated in the smooth border. Thoracic cavity tissues at Ω area have invariable positive limited coefficient of specific conductance.

According to this model, electric potential of the heart $u(x)$ at Ω area is described by the Laplace equation:

$$\Delta u(x) = 0, \tag{1}$$

where $x = (x_1, x_2, x_3)^T \in \Omega \subset R^3$ is a point in 3-D space;

$$\Delta \equiv \frac{\partial}{\partial x_1} + \frac{\partial}{\partial x_2} + \frac{\partial}{x_3}$$

is Laplace operator in the R^3 power.

The Dirichlet condition (potential of electric field measured as the result of surface mapping of ECG) is valid at B_S border at Ω:

$$u(x) = U_0(x),\ x \in B_S. \tag{2}$$

The Dirichlet condition contains noise component (experimental component):

$$U_0(s) = u_0(s) + \xi(s),\ s \in B_S,$$

where $u_0(s)$ is exact potential value at chest surface; $\xi(s)$ is experimental error estimated as $\xi(s) < \delta$.

The Neumann condition is also valid at this border:

$$\frac{\partial u(x)}{\partial n} = P_0(x) = 0, \quad x \in B_S, \tag{3}$$

where $\partial u(x)/\partial n$ is potential derivative $u(x)$ along internal normal to the surface.

The potential $u(x)$ should be harmonized from B_S surface to surface $B_N = B_E \cup B_{T1} \cup B_{T2}$. In other words, potential $u(x)$ trace should be found at the surface B_N. The trace should meet the Laplace condition within area Ω. At the borders of the area the trace should meet the boundary condition described by Eqs. (2)-(3).

In mathematical physics a similar problem is known as the Cauchy problem for the Laplace equation. Boundary conditions (2)-(3) are called Cauchy conditions. According to Hadamard, the Cauchy problem for the Laplace equation is an incorrectly formulated problem: negligible error in boundary conditions may cause indefinitely large solution error [6, 8]. However, the solution is stable provided that solution $u(s)$, $s \in B_N$ is superimposed with condition $u(s) < C$ or $\|u(s)\|_{L2} < C$, where $|C| < \infty$.

Special regularization algorithms provide numerical solution of IP ECG.

3. Algorithms of Numerical Solution of IP ECG

The hardware–software system implements an iteration algorithm of IP ECG solution. This algorithm is based on the method of boundary elements [3]. This method was described in more detail in [12, 4]. Let us consider this method.

For the function determined within area Ω with Lipschitz boundary B and harmonized within area Ω, the third equation of Green is valid:

$$2\pi u(M) = \int_B g(P) \cdot \frac{1}{R(M, P)} ds - \int_B u(P) \cdot \frac{\partial(1/R(M, P))}{\partial n} ds, \quad M \in B,\ P \in B, \tag{4}$$

where M is a fixed point and P is a sliding point at corresponding surfaces; $R(M, P)$ is the vector from point M to point P; $R(M, P) \equiv |MP|$ is the Euclidean length of vector $R(M, P)$, or distance between points M and P; n is the unit normal vector at point P; g is the normal potential derivative at point P; ds is the differential surface element.

Alternating fixation of immobile point M at surfaces B_S and B_N gives two integral equations based on the Green equation:

$$2\pi u(M) = \int_{B_N} g(P) \cdot \frac{1}{R(M, P)} ds -$$

$$-\int_{B_N} u(P)\cdot\frac{\partial(1/R(M,P))}{\partial n}\,ds+\int_{B_S} g(P)\cdot\frac{1}{R(M,P)}\,ds-$$
$$-\int_{B_S} u(P)\cdot\frac{\partial(1/R(M,P))}{\partial n}\,ds,\ M\in B_S; \qquad (5)$$

$$2\pi u(M)=\int_{B_N} g(P)\cdot\frac{1}{R(M,P)}\,ds-$$
$$-\int_{B_N} u(P)\cdot\frac{\partial(1/R(M,P))}{\partial n}\,ds+\int_{B_S} g(P)\cdot\frac{1}{R(M,P)}\,ds-$$
$$-\int_{B_S} u(P)\cdot\frac{\partial(1/R(M,P))}{\partial n}\,ds,\ M\in B_N. \qquad (6)$$

Values $2\pi u(M)$, $M \in B_S$, as well as integrals over surface B_S, can be determined. Grouping of known functions gives a set of simultaneous Fredholm equations I and II with respect to functions u and g at surface B_N.

To solve this set of simultaneous integral equations using the boundary element method, let the surface $B = B_S \cup B_N$ be divided into elements ω_i:

$$B=\cup_{i=1}^{N}\omega_i.$$

Potential $u(s)$ and normal derivative $g(s)$ can be represented as deconvolution of linear independent basis functions $\varphi_i(s)$:

$$u(s)=\sum_{i=1}^{N} u_i\cdot\varphi_i(s);$$
$$g(s)=\sum_{i=1}^{N} g_i\cdot\varphi_i(s), \qquad (7)$$

where deconvolution coefficients u_i and g_i are potential $u(s)$ values and its normal derivative $g(s)$ at gravity centers of boundary elements ω_i.

Basis functions φ_i are represented by piecewise constant functions determined as:

$$\begin{cases}\varphi_i(s)=1, s\in\omega_i;\\ \varphi_i(s)=0, s\notin\omega_i.\end{cases}$$

This scheme is a simple variant of the boundary element method. Piecewise linear polynomials and nonlinear functions can be used as basis functions to increase calculation accuracy. Substitution of Eq. (8) into Eqs. (6)-(7) with regard to Eq. (3) gives a set of simultaneous matrix-vector equations:

$$\begin{bmatrix}-H^{NN} & G^{NN}\\ -H^{SN} & G^{SN}\end{bmatrix}\cdot\begin{bmatrix}u^N\\ g^N\end{bmatrix}=\begin{bmatrix}H^{NS}\cdot u^S\\ H^{SS}\cdot u^S\end{bmatrix}, \qquad (8)$$

where matrices $H^{i,j}$ and $G^{i,j}$ have the following structure:

$$H^{i,j}\equiv\left[h_{m,p}^{i,j}\right]=\int_{\omega_p}\frac{R_{m,p}^{i,j}\cdot n}{\left|R_{m,p}^{i,j}\right|^3}, i\neq j, m\neq p;$$

$$H^{i,j}\equiv\left[h_{m,p}^{j,j}\right]=\int_{\omega_p}\frac{R_{m,p}^{i,j}\cdot n}{\left|R_{m,p}^{i,j}\right|^3}+2\pi, i=j, m=p;$$

$$G^{i,j}\equiv\left[g_{m,p}^{i,j}\right]=\int_{\omega_p}\frac{1}{R_{m,p}^{i,j}}\,ds, \qquad (9)$$

where ω_p is boundary element with index p at surface B_j; $R_{m,p}^{i,j}$ is vector directed from center of gravity of boundary element with index m to surface B_i and from center of gravity of boundary element with index p to surface B_j.

Vectors u^j and g^j have the following structure:

$$u^j=(u_1^{\,j}, u_2^{\,j}, \ldots u_p^{\,j}, \ldots u_N^{\,j})^T;$$
$$g^j=(g_1^{\,j}, g_2^{\,j}, \ldots g_p^{\,j}, \ldots g_N^{\,j})^T, \qquad (10)$$

where u_p^j and g_p^j are functions $u(s)$ and $g(s)$ in boundary element with index p at surface B_j.

Numerical solution of the set of simultaneous equations (9) can be found using various methods. The hardware–software system implements the Seidel iteration algorithm (9). This algorithm allows the solution to be more accurate than solution obtained using direct conventional methods. Iteration procedure is:

$$g^{(1)}=g_0;$$
$$u^{(2k)}=(H^{NN})^{-1}\cdot(G^{NN}g^{(2k-1)}-c_2);$$
$$g^{(2k+1)}=(G^{SN})^{-1}\cdot(H^{SN}u^{(2k)}+c_1), \qquad (11)$$

where g_0 is initial approximation; $k = 1, 2, \ldots, n$ are numbers of iteration stages.

Iteration efficiency requires calculation of the product $(H^{NN})^{-1}\cdot G^{NN}$; $(H^{NN})^{-1}\cdot c_2$, $(G^{SN})^{-1}\cdot H^{SN}$; $(G^{SN})^{-1}\cdot c_1$. Further, matrix multiplied by vector should be used. This increases the rate of algorithm calculation.

The number of iteration steps is calculated using the principle of the residual (Morozov principle): the procedure is stopped at stage 2N. Then the residual norm is equal to normal error of the free term:

$$|H^{NN} \cdot u^{(2N)} - G^{NN} \cdot g^{(2N-1)} + c_2| \le |H^{NS}| \cdot \delta, \qquad (12)$$

where δ is electric field potential error at the chest surface.

Inverse matrices should be calculated to implement the iteration procedure: $(H^{NN})^{-1}$ and $(H^{SN})^{-1}$. Square matrix H^{NN} is substantially determined. Therefore, this matrix can be addressed directly. Matrix H^{SN} is square if the numbers of boundary elements at each surface B_N and B_S are equal to each other. These surfaces have different areas and their triangulation using equal number of elements would give significant spread in the boundary element size. This decreases calculation accuracy. In this work the matrices are not square. The matrix H^{SN} is poorly determined and regularization algorithms should be used to inverse this matrix. The Tikhonov method was used to calculated pseudoinverse H^{SN} matrix:

$$A_\alpha^{+} = (A^{\mathrm{T}}A + \alpha E)^{-1}A^{\mathrm{T}},$$

where α is regularization parameter calculated using the principle of the residual. In tests the algorithm converged within 30-45 iterations with relative error of level 10^{-3}-10^{-2}.

4. Hardware–Software System Architecture and Main Stages of Noninvasive EPE of the Heart

The hardware–software diagnostic system is based on computer software for Windows XP. The hardware–software diagnostic system is compatible with industrial system for surface ECG mapping Cardiag 128.1 and helical computer tomographic scanners Imatron C-150, etc. The hardware–software diagnostic system uses a set of surface ECG records in MAP Cardiag format and chest tomograms in standard format DICOM as input data.

The software includes the following components.

1. Preprocessor for input data preprocessing implementing C/C++ language.

2. Computation processor for IP ECG solution in the Matlab 7 medium.

3. Postprocessor for interactive visualization of examination data based on Java language using Open GL libraries.

The hardware–software system capacity includes the following.

1. Construction and visualization of realistic 3-D computer models of thoracic cavity and heart.

2. Interactive reconstruction of epicardial monopolar and bipolar electrograms at given points on the heart surface.

3. Plotting of isochronous maps of cardiocycle using realistic 3-D models of the heart.

4. Plotting of isochronous maps of cardiocycle using realistic 3-D models of the heart in automatic and manual modes.

5. Animation-mode visualization of depolarization and repolarization dynamics of the myocardium.

The diagnosis process falls into the following stages.

1. *ECG surface mapping.* ECG mapping at the chest surface is implemented using the Cardiag 128.1 system. ECG mapping at the chest surface includes synchronous ECG detection in 80 unipolar leads at the chest surface and 3 standard leads at the patient's extremities.

Disposable Ag/Cl electrodes were used for ECG mapping (electrodes for ECG daily monitoring). Chest electrodes were arranged as 5 belts at levels I, III, V, VII, IX of ribs near sternum. Each belt included 16 electrodes uniformly distributed over the chest surface. ECG was detected in the supine patient with upward elevated arms, i.e., in position of chest tomogram detection.

Mapping procedure includes electrode application, signal quality control in each lead, multichannel ECG recording for 10-15 sec with held breath, program filtration of ECG signal, and selection of the cardiocycle of interest from the record.

Surface ECG mapping results in MAP files containing digital ECG in 80 leads at the chest surface. The signal noise is filtered and isoline is normalized.

2. *Computer tomography of thoracic cavity and heart.* Helical computer tomography of the thoracic cavity is performed after surface ECG monitoring with surface electrodes. The step of the helix is 5-7 mm or 3 mm for scanning of thoracic cavity or heart, respectively. Scanning mode is ECG synchronization. Computer tomography gives tomograms of thoracic cavity and heart in DICOM digital format.

3. *Data preprocessing.* Automatic processing of computer tomography data gives thoracic cavity outline and coordinates of surface electrodes. Thoracic cavity cross-sections are closed spline curves providing basis of NURBS-model of thoracic cavity surface.

The heart model is plotted semi-automatically with operator contribution. The Voxel model of the heart is plotted first. The operator edits this model using a 3-D editor program. The NURBS-model of the heart surface is plotted automatically. NURBS-models of thoracic cavity and heart give rise to triangulation border networks described in [5].

Coordinates of ECG electrodes allow ECG surface maps to be normalized. Isopotential maps are plotted. This gives heart electric field potentials at nodules of the thoracic cavity network. Electric potential interpolation at

the chest surface was performed using the method of harmonic interpolation suggested by L. I. Titomir et al. [7].

The preprocessing results are stored in an IPC file containing a list of 3-D coordinates of triangulation network nodules of boundary elements of the heart surface and the body surface. This file also contains heart electric field potentials at each cardiocycle stage at the body surface nodules.

4. *IP ECG solution*. Preprocessing data can be used in IP ECG solution at any cardiocycle stage. The algorithm considered above can be used in IP ECG solution. Sets of simultaneous matrix-vector equations (8) are constructed first. Sets of simultaneous matrix-vector equations (8) are constructed using Eqs. (9)-(10). The sets of simultaneous matrix-vector equations (8) are solved using an iteration method and equations (11).

This gives potentials of electric field of the heart at any cardiocycle stage in heart surface nodules. These data are stored in IPC format file.

5. *Data post-processing*. Data are visualized as isopotential or isochronous activation maps in realistic heart model or as reconstructed epicardial ECG. Potentials are calculated at any point of the model of the heart and body using bilinear interpolation in boundary nodules. Monopolar ECG is reconstructed using linear interpolation at any discrete moment of the cardiocycle. The reconstruction point is selected in interactive mode using a mouse. Isochronous maps are plotted automatically or manually. Manual plotting is preceded by time point selection in bipolar or monopolar ECG records.

5. Results of Clinical Tests

Noninvasive epicardial mapping can be verified using invasive epicardial mapping based on transpericardial access. This procedure is technologically sophisticated.

An approach to quantitative verification of potential reconstruction accuracy is to use intra-esophageal electrograms. The esophagus directly contacts the left atrium posterior wall and is close to the left ventricle. Intra-esophageal electrograms are similar to epicardial electrograms recorded at heart surface points close to the esophagus.

Comparison between reconstructed and intra-esophageal electrograms revealed close similarity between

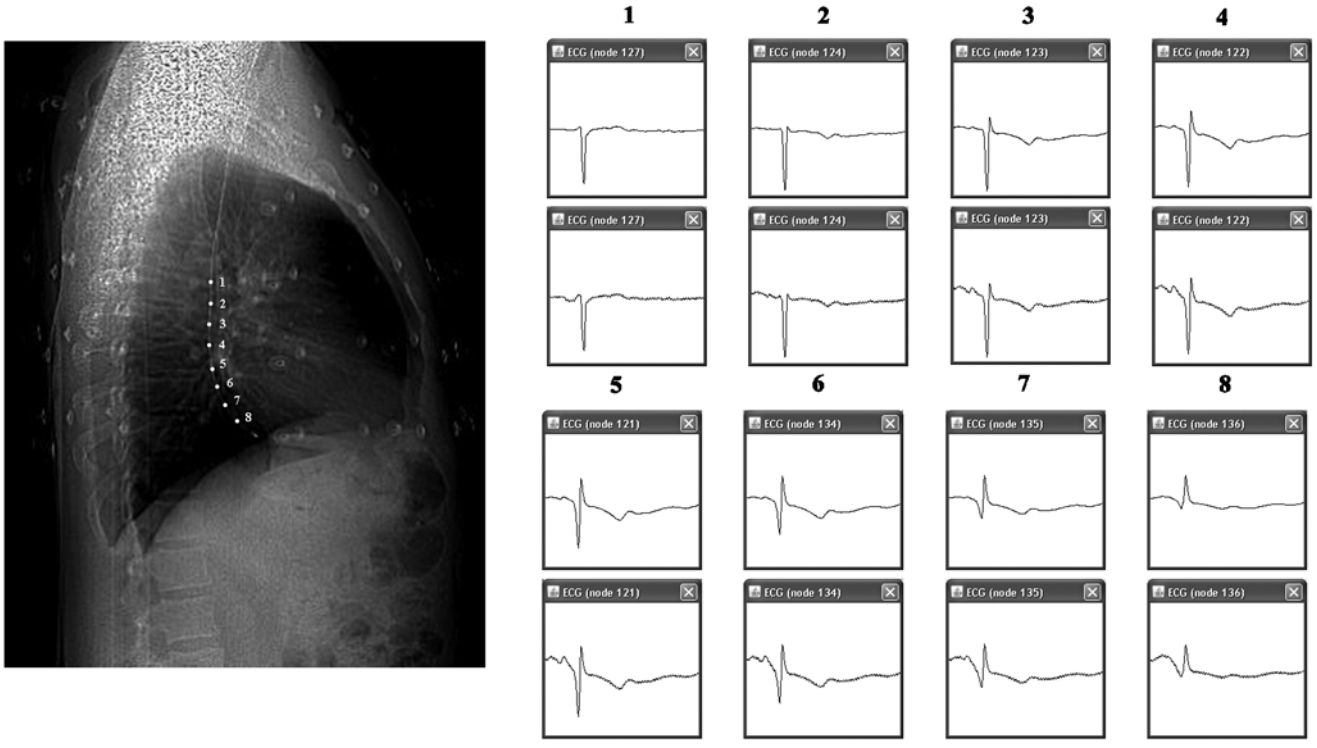

Fig. 1. An example of reconstruction of intra-esophageal electrograms: left – reconstruction of right lateral X-ray projection of thoracic cavity, electrodes of intra-esophageal probe are marked; right – reconstructed (top row) and experimental (bottom row) intra-esophageal electrograms.

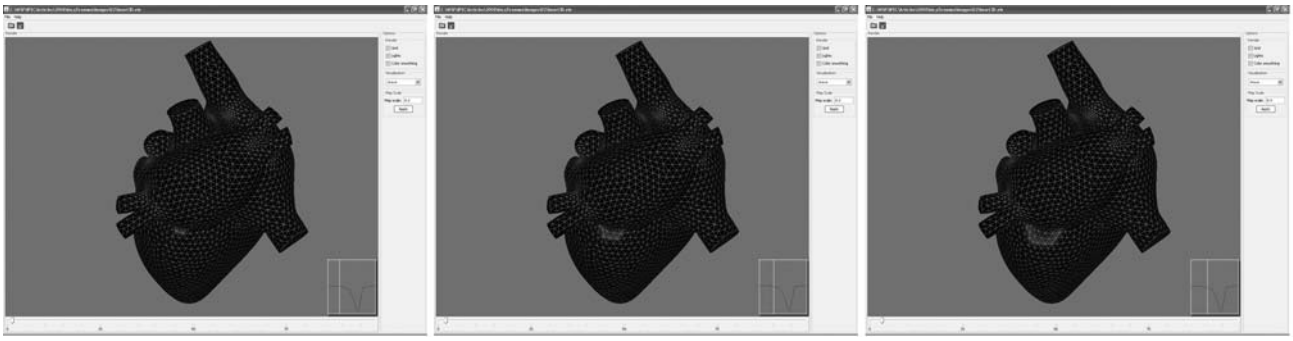

Fig. 2. Reconstruction of myocardium depolarization dynamics in a patient with left lateral syndrome WPW.

the electrograms (Fig. 1). Mean square error of reconstruction was 7%. Noise level of experimental electrograms (signal deviation from zero within interval P-Q) was 0.5 mV (3-4% of maximal signal amplitude). Numerical reconstruction provides sufficiently accurate intra-esophageal electrographic signals comparable with error of experimental signals.

Accuracy of ectopic source localization can be tested using noninvasive isopotential and isochronous maps. Endocardial electrode of implanted pacemaker was used as model source. The stimulation electrode was fixed and its localization error was equal to computer tomograph resolution.

Early activation area determined from reconstructed epicardial maps coincided with site of fixation of the endocardial electrode. Distance from endocardial electrode projection point to early activation point was 3 mm.

Promising results were obtained in patients with manifested syndrome WPW (Fig. 2). Zones of early myocardium activation at atrioventricular furrow and myocardium depolarization dynamics coincided with results of invasive electro-anatomical mapping in a CARTO system. Pre-surgical localization of additional conductive pathways excluded search procedure during surgical intervention.

Zones of early myocardium activation were also localized in patients with non-coronary ventricular ectopic arrhythmias (Fig. 3). All patients demonstrated satisfactory coincidence of ectopic source localization with true localization supported by invasive mapping data and radiofrequency ablation.

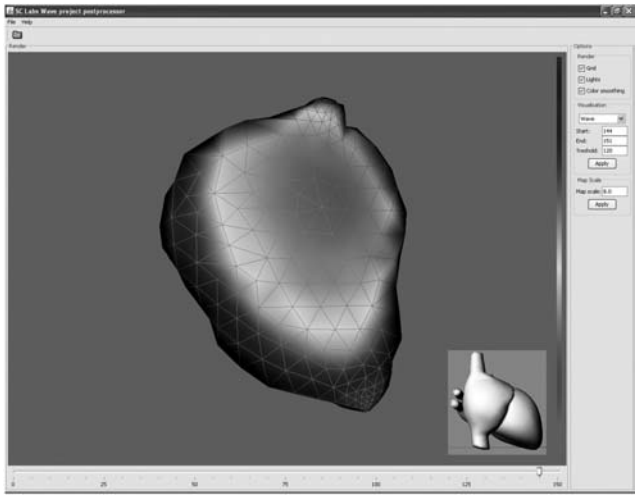

Fig. 3. Isochronous map of right surface of inter-ventricular septum with ectopic source in frontal top part.

6. Conclusion

Clinical tests of the hardware–software system for noninvasive electrocardiographic examination of the heart demonstrated its efficiency for topical diagnosis of cardiac arrhythmia. This system is promising for pre-surgical examination of patients before surgical intervention.

Further upgrade of the hardware–software system and method of noninvasive electrocardiographic examination of heart can be implemented in the following directions.

1. Surface ECG mapping using a large number of chest leads; increase in signal/noise ratio of surface ECG records.

2. Increased accuracy and anatomical credibility of 3-D heart models used for mapping.

3. Regard to different electric conductance of organs and tissues in heart model reconstruction. This would increase the accuracy of noninvasive electrocardiographic examination of the heart.

REFERENCES

1. R. C. Barr and M. S. Spach, Inverse Solutions Directly in Terms of Potentials [Russian translation], Meditsina, Moscow (1979).
2. L. A. Bokeriya, Tachyarrhythmias: Diagnosis and Surgical Treatment [in Russian], Meditsina, Moscow (1989).
3. C. A. Brebbia, J. C. Telles, and L. Wrobel, Boundary Element Techniques [Russian translation], Mir, Moscow (1987).
4. A. Sh. Revishvili, V. V. Kalinin, O. A. Lyadzhina, and E. A. Fetisova, Vestn. Aritmol., No. 51 (2008).
5. E. R. Gol'nik, A. A. Vdovichenko, and A. A. Uspekhov, Inf. Tekhnol., No. 4 (2004).
6. A. M. Denisov, Introduction to the Inverse Problem Theory [in Russian], MGU, Moscow (1994).
7. L. I. Titomir, V. G. Trunov, and E. A. I. Aidu, Noninvasive Electrocardiography [in Russian], Nauka, Moscow (2003).
8. A. N. Tikhonov and V. Ya. Arsenin, Methods for Solution of Incorrect Problems [in Russian], Nauka, Moscow (1986).
9. V. V. Shakin, Computational Electrocardiography [in Russian], Nauka, Moscow (1981).
10. T. Berger, G. Fisher, B. Pfeifer, et al., J. Am. Coll. Cardiol., **48** (2006).
11. R. S. MacLeod and D. H. Brooks, IEEE Eng. in Med. Bio. Mag., **17**, No. 1 (1998).
12. C. Ramanathan, R. N. Ghanem, P. Jia, K. Ryu, and Y. Rudy, Nature Med., **10** (2004).